

光学学报

基于钯修饰六方氮化硼的光纤氢气传感器

丁晖, 郭茂森*, 徐浩东, 韩春阳, 陈宸

西安交通大学电气工程学院, 陕西 西安 710049

摘要 氢气作为一种可持续、无污染的新型绿色能源,在现代工业中受到了广泛关注。但在存储和使用过程中,氢气容易发生泄漏并引发爆炸,因此对其体积分数进行检测非常重要。为此,提出一种基于钯(Pd)修饰六方氮化硼(hBN)薄膜的新型探针式光纤氢气传感器。讨论hBN薄膜的机械和光学特性,指出其作为Fabry-Perot(F-P)干涉仪反射膜在机械、光学、氢气吸附/脱附速度等领域所具有的显著技术优势;研究hBN表面敷Pd的工艺过程;设计以Pd修饰hBN薄膜为反射膜的光纤F-P腔结构并研究其制备工艺。实验结果表明,所设计的传感器在氢气体积分数为0.02%~0.5%时的检测灵敏度为 $0.58 \text{ pm}/10^{-6}$,对体积分数为0.1%的氢气的响应时间为60 s,且具有重复性好等特点。该传感器结构紧凑、耐腐蚀,在电力变压器油中氢气检测等方面具有潜在的技术优势。

关键词 传感器; 氢气体积分数; 氮化硼; Fabry-Perot干涉; 在线测量

中图分类号 TP212 文献标志码 A

DOI: 10.3788/AOS230964

1 引言

能源危机和生态问题不断促使人类寻找新型清洁能源来代替传统化石燃料。氢气(H_2)作为一种绿色的可再生能源,因优异的燃烧性能和无污染特性受到了大量关注,在化学、生物医学和航空航天领域有着广泛应用^[1-3]。然而氢气也是一种易挥发、易燃、易爆气体,当空气中氢气体积分数超过4%时,极易发生爆炸^[4-5],在其存储、运输和使用过程中面临较大的风险,因此安全可靠地检测氢气体积分数是预防爆炸事故发生的有效途径。

与电学类传感器相比,光纤传感器具有体积小、抗电磁干扰和本质安全等优点^[6-8],适用于易燃易爆环境中对氢气体积分数的检测,因此受到了广泛关注。按照检测原理的不同,光纤氢气传感器分为光栅型^[9-10]、倏逝场型^[11-12]、表面等离子共振型^[13-14]和干涉型^[15-16]等几类。其中光纤光栅型氢气传感器利用敷钯光栅在吸附氢气后波长的改变实现对氢气体积分数的检测,具有分布式测量等优点,但受限于光纤自身材质,检测灵敏度较低,一般为几十 $\text{pm} \cdot \%^{-1}$ ^[17]。基于倏逝场和表面等离子共振(SPR)原理的光纤氢气传感器一般利用钯与氧化锌等复合敏感材料在吸附氢气后折射率的变化实现对外界氢气的测量,该类氢气传感器灵敏度较高,可达 $7.5 \text{ nm} \cdot \%^{-1}$ ^[18]。但倏逝场型传感器通常需要对光纤进行拉锥或刻蚀处理,影响了传感器的稳定性,

而SPR型光纤氢气传感器的氢气敏感膜通常为多层结构,制备工艺和过程较为繁琐,不利于实际应用。基于F-P干涉的光纤氢气传感器因机械结构稳定、制作工艺简单而成为干涉型氢气传感器的典型结构。F-P腔型光纤氢气传感器的检测性能主要取决于氢敏薄膜的机械、光学、热学等参数。目前研究人员将Pd修饰二氧化硅^[19]和聚合物^[20]等敏感薄膜作为F-P腔的反射膜。这里,F-P腔氢气传感器的敏感膜一般包括衬底层和敷钯层两部分。研究表明:敷钯层和衬底层的厚度共同决定了传感器的响应速度,二者的厚度越薄,传感器响应速度越快。其中敷钯层的厚度又是决定传感器响应灵敏度的主要因素。实际制作中,敷钯层的厚度可以通过制备工艺过程得到一定程度的控制,而衬底层厚度受制备工艺、材料的机械强度等多种因素限制,很难在保证机械强度的同时达到理想的厚度。目前常用的聚合物、二氧化硅等衬底材料厚度通常为几微米或几十微米量级;不带衬底材料的纯Pd膜可以达到几十纳米厚度^[21];基于二维材料石墨烯^[22]的氢敏薄膜厚度为纳米级,在氢气体积分数为0.5%时传感器的响应时间为18 s,相比其他衬底材料,明显提高了传感器的响应速度。

综上,研究制备厚度更薄并具有较好机械特性的氢敏感膜是F-P腔型氢气传感器所需解决的关键问题。为此,本文提出一种基于Pd修饰多层hBN薄膜的光学氢气传感器。多层hBN薄膜厚度仅为纳米级,

收稿日期: 2023-05-10; 修回日期: 2023-06-26; 录用日期: 2023-07-04; 网络首发日期: 2023-08-02

基金项目: 国家自然科学基金面上项目(51777150)、国家自然科学基金青年科学基金项目(51907146)

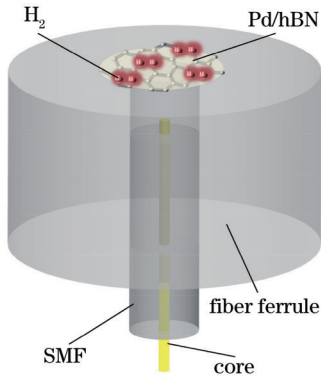
通信作者: *maosenguo@stu.xjtu.edu.cn

但机械强度很高且表面极少有悬挂键和电荷陷阱的存在。同时, hBN具有较好的化学惰性和极低的热膨胀系数, 因此是承载Pd的良好衬底。相比石墨烯, hBN是绝缘体且杨氏模量更低, 在相同应力下hBN薄膜产生的形变量相比同尺寸的石墨烯薄膜更大, 因此利用hBN作为Pd的衬底材料可使传感器具有更高的检测灵敏度。本文分析了基于Pd修饰hBN薄膜的F-P腔氢气传感器的敏感机理, 讨论了Pd修饰hBN薄膜在氢气敏感方面的优势, 研究了传感器制备工艺并实现了传感器制备, 最后对传感器性能进行了实验室测试。实验结果表明, 相比传统氢气传感器, 基于Pd修饰hBN薄膜的氢气传感器在消除“响应记忆”、提升检测灵敏度和缩短响应时间等方面具有更优的性能。所设计的传感器在电力变压器油中氢气检测等方面具有潜在的技术优势。

2 氢气传感检测原理

2.1 基于hBN薄膜的F-P干涉仪设计

Pd修饰多层hBN薄膜的光学氢气传感器结构如图1所示。借助平整的光纤端面与Pd/hBN薄膜形成柔性F-P干涉仪。当Pd吸附氢气时会膨胀, 从而拉伸hBN薄膜使其产生形变, 进而改变干涉仪的腔长, 引起干涉光谱漂移, 因此可通过测量光谱的漂移量实现微量氢气传感。



SMF: single mode fiber

图1 基于Pd修饰多层hBN薄膜的光学氢气传感器结构示意图

Fig. 1 Schematic of optical hydrogen sensor based on Pd-decorated multilayer hBN film

2.2 传感器氢气敏感机理分析

当Pd/hBN复合膜暴露于H₂环境中时, 其表面吸附H₂分子并将其解离为氢原子, 氢原子通过扩散作用迅速进入Pd内部, 形成PdH_x间隙固溶体, 直到达到平衡^[23-24]。当外界H₂浓度降低时, Pd中的氢原子在Pd表面结合成H₂并脱附, 此反应为可逆反应, 反应方程式为



密度泛函理论(DFT)计算方法已证明PdH_x的形成会导致Pd晶格膨胀, 从而Pd产生的应变 ϵ_{Pd} ^[25]可以表示为

$$\epsilon_{\text{Pd}} = 0.026 \frac{\sqrt{P_{\text{H}_2}}}{S} \quad (2)$$

式中: P_{H_2} 为外界环境的氢气分压, S 为Sievert系数($S = 46.66 \text{ kPa}^{1/2}$)。Pd产生的应变 ϵ_{Pd} 会拉伸衬底hBN薄膜, 假设Pd/hBN复合膜是有弹性的, 则复合膜产生的应变 ϵ_c ^[22]表示为

$$\epsilon_c = \frac{E_{\text{Pd}} h_{\text{Pd}}}{E_{\text{Pd}} h_{\text{Pd}} + E_{\text{hBN}} h_{\text{hBN}}} \epsilon_{\text{Pd}} \quad (3)$$

式中: E_{Pd} (E_{hBN})和 h_{Pd} (h_{hBN})分别是Pd(hBN)膜的杨氏模量和厚度。Pd/hBN复合膜的应变会使其发生向下形变, 如图2所示, 使干涉仪腔长减小 ΔL , 进而干涉光谱发生漂移 $\Delta\lambda$, 两者遵循的关系^[26]为

$$\frac{\Delta\lambda}{\lambda} = \frac{\Delta L}{L} \quad (4)$$

式中: λ 是干涉光谱波谷处波长; L 是F-P腔的初始长度。因此可以通过测量干涉光谱的波长漂移量来提取外界氢气浓度。式(1)为可逆反应, 因此当外界H₂浓度降低时, 上述过程发生逆转, 干涉光谱恢复至原始位置。

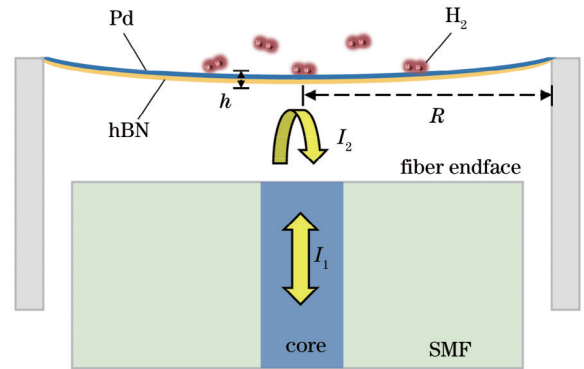


图2 氢气检测原理示意图

Fig. 2 Schematic of hydrogen detection principle

2.3 传感器响应灵敏度分析

通过上述分析可知, Pd/hBN复合膜吸附H₂后产生的形变量越大, 传感器的灵敏度越高, 当外界H₂分压一定时, 复合膜的厚度和半径等参数决定了形变量的大小。因此, 通过合理的参数设计可以使传感器获得较高的灵敏度。如图2所示, hBN作为Pd的衬底可视为边界固定的圆形薄膜, 假设Pd膨胀产生的应力 σ_{Pd} 均匀作用于hBN薄膜, 则圆形hBN薄膜的形变量 d ^[27]可以表示为

$$d = \frac{3\sigma_{\text{Pd}}(1-\mu^2)}{16Eh^3} (R^2 - r^2) \quad (5)$$

式中: μ 、 E 、 h 和 R 分别为hBN薄膜的泊松比(0.16)、杨氏模量(0.8 TPa)、厚度和半径; r 为薄膜各点距中心点的间距。通过式(5)仿真计算了厚度为4 nm、半径

为 $100\ \mu\text{m}$ 的圆形 hBN 薄膜在应力作用下不同位置的形变量变化,结果如图 3 所示,膜片边界处产生的形变量较小,而距离膜片中心点越近的位置产生的形变量越大。

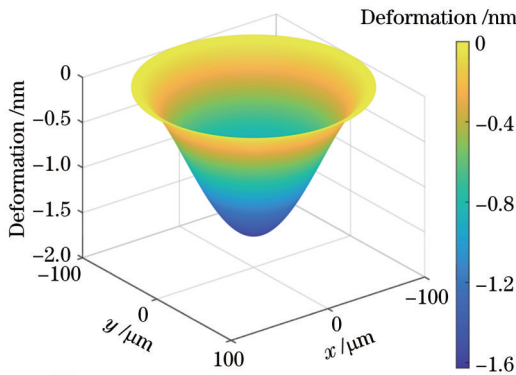


图 3 应力作用下薄膜不同位置处的形变量

Fig. 3 Deformation of diaphragm at different positions under pressure

因此在传感器制备过程中,应保证光纤对准薄膜中心位置。当只考虑中心点即 $r=0$ 时,薄膜形变量与厚度和半径相关,如图 4 所示。从图 4 可知,在应力一定时,半径 R 越大、厚度 h 越薄的薄膜其中心点的形变量越大,且半径的变化对形变量的影响要大于厚度。从式(5)还可看出:假设外界应力和薄膜尺寸一定,材料的泊松比和杨氏模量越小,形变量越大。hBN 的泊松比与其他二维纳米材料接近,但杨氏模量相较于其他纳米材料如石墨烯($1\ \text{TPa}$)更低。因此相比相同尺寸参数的石墨烯薄膜,hBN 薄膜作为衬底可获得更大的形变量,进而提升传感器的检测灵敏度。

通过以上分析可知,应尽可能选择较薄的 hBN 薄膜并合理设计支撑结构,令其具有合适的半径,从而使传感器具有较高的灵敏度。但超薄的单层 hBN 薄膜在传感器制备过程中晶格结构容易破损,且半径过大会降低衬底 hBN 的稳定性和机械性能,使 Pd/hBN 敏

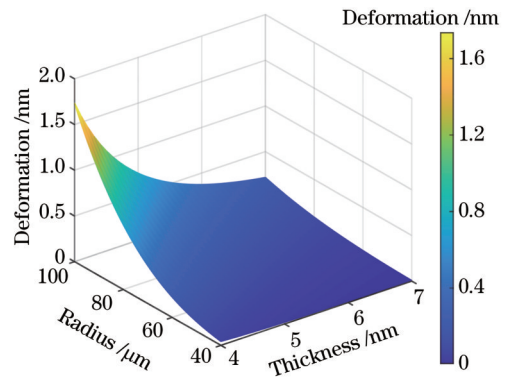


图 4 中心点形变量与薄膜几何参数之间的关系

Fig. 4 Relationship between the central point deformation and the geometric parameters of the diaphragm

感薄膜形变后难以恢复至初始位置,引入“响应记忆”等问题。因此,综合考虑各方面因素,最终选择多层 hBN 薄膜($\sim 5\ \text{nm}$ 厚度)作为衬底,设计半径为 $62.5\ \mu\text{m}$ 。hBN 表面敷 Pd 厚度不宜过厚,较厚的 Pd 膜会增加传感器的响应时间^[22,28],同时对衬底的应力过大,易使 hBN 膜发生破裂,导致传感器无法工作。经过反复实验测试,认为 Pd 膜厚度应当控制在 $10\ \text{nm}$ 以内。

3 氢气传感器制备

氢气传感器的制备步骤如图 5 所示,可分为以下步骤。1)将铜基多层 hBN 薄膜浸入 FeCl_3 溶液中,用以刻蚀铜衬底;2)将去除衬底的 hBN 薄膜转移至去离子水中,以洗掉残存的铁离子;3)为了便于薄膜转移和光纤固定,并保证光纤对准悬空薄膜的中心点,选择光纤插芯作为薄膜的支撑结构,利用 hBN 薄膜优异的机械特性将其从水溶液转移至插芯端面;4)将敷有 hBN 薄膜的插芯在室温下垂直放置 $24\ \text{h}$,待水分蒸发后由于范德瓦耳斯力的作用^[29],hBN 薄膜会牢固地粘贴在插芯表面;5)磁控溅射相比其他镀膜技术可以在低温

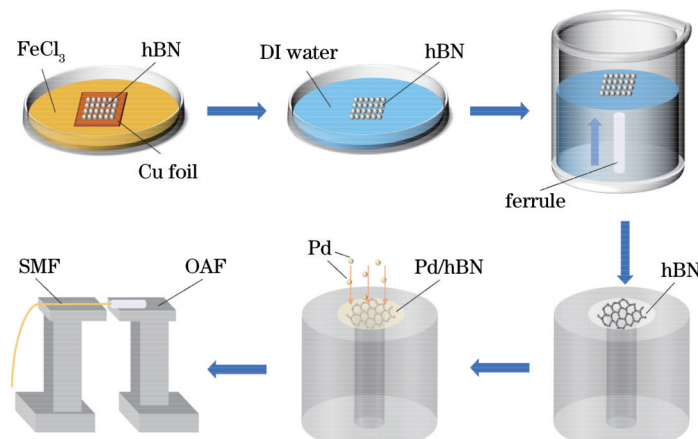


图 5 基于 Pd 修饰 hBN 薄膜的光学氢气传感器制备过程示意图

Fig. 5 Schematic of optical hydrogen sensor preparation based on Pd-decorated hBN film

的条件下实现高速沉积,对基片的损伤小且溅射所得的薄膜与基片结合较好,通过调控溅射功率和溅射时间可以控制镀膜厚度。利用磁控溅射技术在 hBN 薄膜表面沉积一层 Pd,其厚度约为 5 nm;6)利用光学调节架将光纤与敏感膜对准,最佳对准效果可以通过观察干涉光谱获得,最后使用环氧树脂胶进行固定。

图 6 为最终制备的传感器的输出光谱。自由光谱范围(FSR)为 6.4 nm,干涉条纹对比度为 16 dB。图 6 中插图为制备完成的传感器实物图,该传感器体积小,结构紧凑。

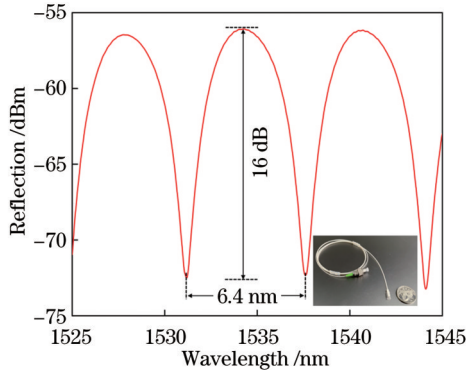


图 6 光学氢气传感器的初始反射光谱

Fig. 6 Initial reflection spectrum of optical hydrogen sensor

4 实验结果与分析

4.1 实验装置

搭建实验平台用以对氢气传感器进行测试和标定,平台结构如图 7 所示。采用带宽为 40 nm 的宽带光源(BBS)作为输入光,通过 AQ6370B 型光谱分析仪(OSA)观察反射光谱。氢气传感器被水平放置于气

室中,通过两个质量流量控制计(MFC)来调控混合气体中氢气和空气的体积比,从而控制通入测量气室中的氢气体积分数,实现不同氢气体积分数下传感器响应的测量。

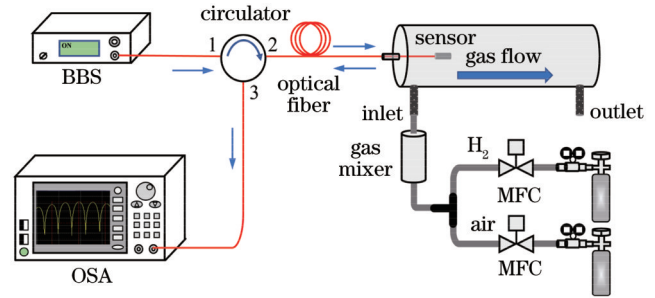


图 7 氢气传感器测试平台示意图

Fig. 7 Schematic of the hydrogen sensor detection platform

4.2 传感器吸氢/脱氢过程光谱变化

氢气吸附过程传感器光谱的变化。首先向测量气室内通入体积分数为 0.10% 的氢气,每间隔 5 s 观察并记录传感器吸附氢气过程中反射光谱的变化,结果如图 8(a)所示。由图 8(a)可知,在吸氢过程中,传感器光谱发生了蓝移。在通入 0.10% 体积分数氢气前 20 s 内光谱蓝移速度较快,之后光谱蓝移速度逐渐减慢,最终经过 85 s 后,光谱达到蓝移的最大值并趋于稳定,最终蓝移量 0.65 nm。

氢气脱附过程传感器光谱的变化。向气室内通入空气,每隔 5 s 观察并记录传感器在脱附氢气过程中反射光谱的变化,结果如图 8(b)所示。由图 8(b)可知,在脱氢过程中,传感器光谱发生了红移。在脱氢开始前 25 s 内光谱红移速度较快,之后光谱红移速度逐渐减慢,最终经过 75 s 后,光谱达到红移的最大值并趋于稳定,最终红移量 0.64 nm。

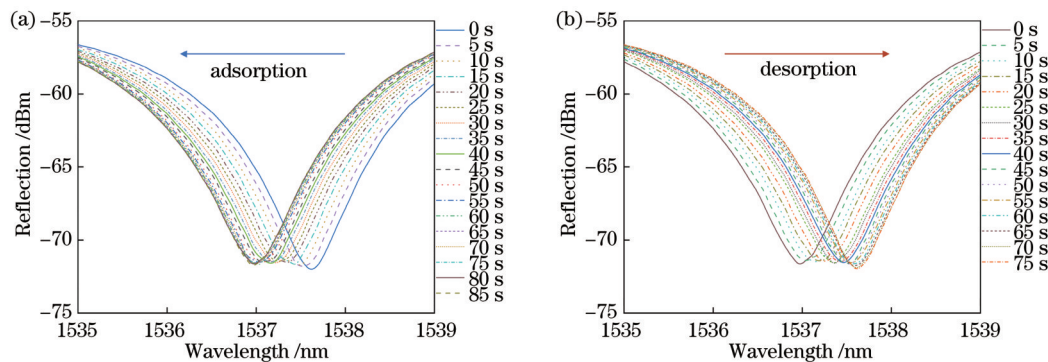


图 8 氢气体积分数为 0.10% 时吸氢/脱氢过程中光谱随时间变化情况。(a)吸附过程;(b)脱附过程

Fig. 8 Spectra of adsorption and desorption process varying with time at 0.10% H_2 volume fraction. (a) Adsorption process; (b) desorption process

通过观察传感器反射光谱在吸氢和脱氢时的漂移情况,证明了传感器对氢气具有较好的敏感特性。同时,在氢气吸附和脱附过程中,传感器光谱的蓝移量与红移量基本一致。这是因为 hBN 极高的杨氏模量使

得 Pd/hBN 薄膜具有很好的刚性,从而保证了传感器无“响应记忆”问题。此外,具有大比表面积和纳米厚度的 Pd/hBN 薄膜有助于氢气的快速吸附、解离以及脱附。从图 8 中可得出,针对体积分数为 0.10% 的氢

气,传感器响应时间和恢复时间为 60 s。当增加待测氢气体积分数时,传感器的响应时间会进一步缩短。

4.3 氢气传感器定量测试

利用光谱仪分别记录了氢气体积分数为 0、0.02%、0.05%、0.10%、0.20%、0.30%、0.40% 和 0.50% 时传感器响应稳定的反射光谱,结果如图 9 所示。从图 9(a)中可以得知:在氢气体积分数从 0 逐渐增加至 0.50% 的过程中,氢气传感器的反射光谱逐渐

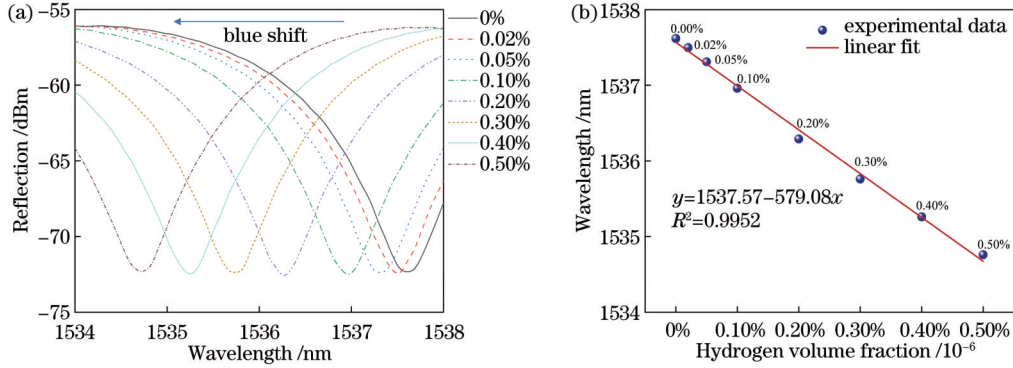


图 9 传感器定量测试结果。(a)不同氢气体积分数下的反射光谱;(b)波谷波长与氢气体积分数的关系

Fig. 9 Sensor quantitative test result. (a) Reflection spectra at different H₂ volume fraction; (b) dip wavelength versus the hydrogen volume fraction

4.4 氢气传感器重复性测试

进一步测试该氢气传感器的重复性和抗疲劳性,进行了 3 次氢气体积分数为 0.10% 的循环实验。氢气传感器反射光谱波长漂移量随时间的变化情况如图 10 所示,单次光谱采集时间间隔 5 s。从实验结果可知:3 次循环实验反射光谱波长的变化趋势相同且对应的光谱蓝移量分别为 0.65 nm、0.66 nm 和 0.64 nm,传感器响应时间均在 60 s 左右,表明传感器针对同一体积分数氢气的响应基本一致。由此证明,hBN 薄膜的较好刚性和抗疲劳性保证了传感器的重复性,解决了采用传统敏感膜的 F-P 传感器对待测氢气的“响应记忆”的问题。

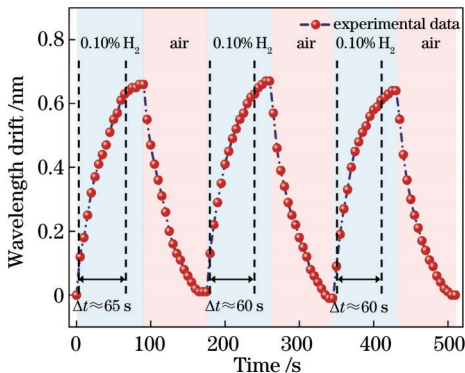


图 10 3 次氢气体积分数为 0.10% 的循环测试

Fig. 10 Three cycle tests with a hydrogen volume fraction of 0.10%

4.5 氢气传感器温度交叉敏感特性研究

在实际应用中,环境温度的大范围波动可能会引

起 Pd/hBN 薄膜形变,从而影响氢气测量结果的准确性。为验证传感器对温度的交叉敏感特性,将传感器水平放置在恒温箱中,将温度从 25 °C 增加至 60 °C,传感器的反射光谱发生了红移,如图 11(a)所示。每个温度保持 5 min 并记录传感器反射光谱波长各 10 次,通过计算得到标准偏差并对实验数据进行线性拟合,结果如图 11(b)所示。通过分析可知,传感器的温度灵敏度为 91 pm/°C,温度交叉敏感度为 0.016 %/°C。hBN 较高的导热系数和极低的热膨胀系数保证了其具有优异的抗热震性能,因此温度的变化对其影响较小。而温度的升高会使环氧树脂胶发生形变,导致光纤位移,从而引起光谱漂移。后期可通过键合或粘合等方法改善传感器的制备工艺,降低温度对传感器的影响,以提高测量精度。

4.6 传感器性能参数对比

表 1 总结了近年来 F-P 型光纤氢气传感器的研究现状,并与所提传感器进行了性能对比。通过比较可知:借助 Pd/hBN 薄膜良好的传感特性,所提传感器具有更高的灵敏度;所提传感器响应时间较长,这是因为实验中所测量的氢气体积分数较低,若进一步提升测量氢气的体积分数,则传感器响应时间会大幅度降低;所提传感器的温度交叉敏感性较高,这主要是因为光纤固定过程中环氧树脂胶的使用导致传感器易受温度影响,通过优化制备工艺及过程可进一步降低传感器的温度敏感性;此外,所提传感器具有较好的重复性和抗疲劳性,制备过程更为简单,成本较低,因此具有巨大的应用潜力。

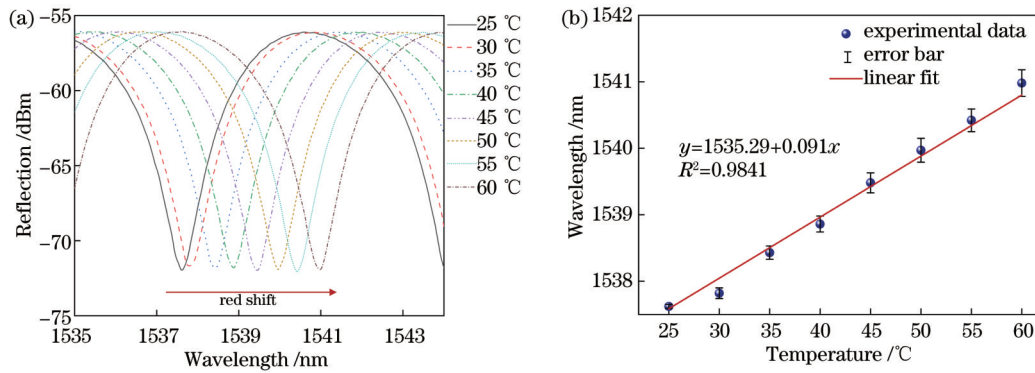


图 11 波长漂移与温度的关系。(a)不同温度下光谱漂移情况;(b)线性拟合结果

Fig. 11 Relationship between wavelength shift and temperature. (a) Spectral drift at different temperatures; (b) linear fitting result

表 1 所提传感器与其他 F-P 型传感器的性能

Table 1 Performance of the proposed sensor and other F-P type sensors

Material of sensing probe	Sensitivity	Response time	Detection limit/ 10^{-6}	Temperature sensitivity	Reference
5.6 nm Pd/3.1 nm graphene	~ 2.5 nm/%	18 s at 0.5% H_2	~ 20	~ 1.4 pm/ $^{\circ}C$	[22]
~ 120 nm Pd/ $3 \mu m$ polymer	~ 2.0 nm/%	13.5 s at 4% H_2		127.59 pm/ $^{\circ}C$	[20]
13 nm Pd/113 nm Au/graphene	64 pm/%	4.3 s at 3.5% H_2		~ 10.2 pm/ $^{\circ}C$	[15]
27.4 nm Pd	~ 0.334 nm/%	10 s at 3.5% H_2		4 pm/ $^{\circ}C$	[21]
~ 5 nm Pd/5 nm hBN	5.8 nm/%	60 s at 0.1% H_2	~ 30	91 pm/ $^{\circ}C$	This work

5 结 论

提出了一种基于 Pd 修饰多层 hBN 薄膜的光学氢气传感器。Pd/hBN 作为 F-P 干涉仪反射膜在机械、光学、氢气吸附/脱附速度等领域具有显著的优势;探究了影响传感器氢气检测灵敏度的因素;研究了传感器的制备工艺并实现了传感器的制备。实验结果表明:传感器响应与氢气体积分数之间存在良好的线性关系,检测灵敏度为 $0.58 \text{ pm}/10^{-6}$;传感器响应时间为 60 s,具有较好的重复性和抗疲劳性,无“响应记忆”等问题。所设计的传感器具有体积小、结构紧凑、抗电磁干扰等特点,在电力变压器油中氢气检测等工程场合具有较好的应用前景。

参 考 文 献

- [1] Hosseini S E, Wahid M A. Hydrogen production from renewable and sustainable energy resources: promising green energy carrier for clean development[J]. Renewable and Sustainable Energy Reviews, 2016, 57: 850-866.
- [2] Møller K T, Jensen T R, Akiba E, et al. Hydrogen-a sustainable energy carrier[J]. Progress in Natural Science: Materials International, 2017, 27(1): 34-40.
- [3] 李嘉丽, 洪婉玲, 赵春柳, 等. 基于阵列波导光栅的光纤法布里-珀罗干涉仪型多点氢气传感器[J]. 光学学报, 2021, 41(13): 1306013.
Li J L, Hong W L, Zhao C L, et al. Multi-point optical fiber hydrogen sensor with Fabry-Perot interferometers using arrayed waveguide grating[J]. Acta Optica Sinica, 2021, 41(13): 1306013.
- [4] Li Y N, Zhao C L, Xu B, et al. Optical cascaded Fabry-Perot interferometer hydrogen sensor based on vernier effect[J]. Optics Communications, 2018, 414: 166-171.
- [5] Zhang Y N, Liu Y X, Shi B F, et al. Lateral offset single-mode fiber-based Fabry-Perot interferometers with vernier effect for hydrogen sensing[J]. Analytical Chemistry, 2023, 95(2): 872-880.
- [6] 辛鑫, 吴永武, 刘慧敏, 等. 一种新的光纤 Bragg 光栅氢气传感器制作方法[J]. 光学学报, 2021, 41(4): 0406002.
Xin X, Wu Y W, Liu H M, et al. A new fabrication method of fiber Bragg grating hydrogen sensor[J]. Acta Optica Sinica, 2021, 41(4): 0406002.
- [7] 周贤, 杨沫, 张文, 等. 基于飞秒激光微加工的 Pt-WO₃膜光纤氢气传感器[J]. 中国激光, 2019, 46(12): 1210001.
Zhou X, Yang M, Zhang W, et al. Fiber hydrogen sensor coated with Pt-WO₃ film based on femtosecond laser micro-processing[J]. Chinese Journal of Lasers, 2019, 46(12): 1210001.
- [8] Zhang X P, Li X T, Zhang X H, et al. Photothermal-assisted hydrogen permeation enhancement[J]. Sensors and Actuators B: Chemical, 2022, 365: 131935.
- [9] Zhou X, Dai Y T, Karanja J M, et al. Microstructured FBG hydrogen sensor based on Pt-loaded WO₃[J]. Optics Express, 2017, 25(8): 8777-8786.
- [10] Dai J X, Ruan H B, Zhou Y C, et al. Ultra-high sensitive fiber optic hydrogen sensor in air[J]. Journal of Lightwave Technology, 2022, 40(19): 6583-6589.
- [11] Li J, Fan R, Hu H F, et al. Hydrogen sensing performance of silica microfiber elaborated with Pd nanoparticles[J]. Materials Letters, 2018, 212: 211-213.
- [12] Cao R T, Wu J Y, Liang G Q, et al. Functionalized PdAu alloy on nanocones fabricated on optical fibers for hydrogen sensing[J]. IEEE Sensors Journal, 2020, 20(4): 1922-1927.
- [13] Cai S S, González-Vila Á, Zhang X J, et al. Palladium-coated plasmonic optical fiber gratings for hydrogen detection[J]. Optics Letters, 2019, 44(18): 4483-4486.
- [14] Semwal V, Gupta B D. Highly selective SPR based fiber optic sensor for the detection of hydrogen peroxide[J]. Sensors and Actuators B: Chemical, 2021, 329: 129062.

- [15] Luo J X, Liu S, Chen P J, et al. Fiber optic hydrogen sensor based on a Fabry-Perot interferometer with a fiber Bragg grating and a nanofilm[J]. *Lab on a Chip*, 2021, 21(9): 1752-1758.
- [16] Wu B Q, Zhao C L, Xu B, et al. Optical fiber hydrogen sensor with single Sagnac interferometer loop based on vernier effect[J]. *Sensors and Actuators B: Chemical*, 2018, 255: 3011-3016.
- [17] Hu X Y, Hu W B, Dai J X, et al. Performance of fiber-optic hydrogen sensor based on locally coated π -shifted FBG[J]. *IEEE Sensors Journal*, 2022, 22(24): 23982-23989.
- [18] Yan H T, Zhao X Y, Zhang C, et al. A fast response hydrogen sensor with Pd metallic grating onto a fiber's end-face[J]. *Optics Communications*, 2016, 359: 157-161.
- [19] Iannuzzi D, Slaman M, Rector J H, et al. A fiber-top cantilever for hydrogen detection[J]. *Sensors and Actuators B: Chemical*, 2007, 121(2): 706-708.
- [20] Xiong C, Zhou J T, Liao C R, et al. Fiber-tip polymer microcantilever for fast and highly sensitive hydrogen measurement[J]. *ACS Applied Materials & Interfaces*, 2020, 12(29): 33163-33172.
- [21] Zhang X H, Li X T, Zhang X P, et al. Optics-mechanics synergistic fiber optic sensor for hydrogen detection[J]. *Optics Express*, 2022, 30(18): 32769-32782.
- [22] Ma J, Zhou Y L, Bai X, et al. High-sensitivity and fast-response fiber-tip Fabry-Pérot hydrogen sensor with suspended palladium-decorated graphene[J]. *Nanoscale*, 2019, 11(34): 15821-15827.
- [23] Wang Y, Sun S N, Chou M Y. Total-energy study of hydrogen ordering in $\text{PdH}_x(0 \leq x \leq 1)$ [J]. *Physical Review B*, 1996, 53(1): 1-4.
- [24] Wu X J, Li Q X, Yang J L. Electronic transport properties of Pd-H junctions between two $\text{PdH}_x(x=0, 0.25, 0.5, 0.75, 1)$ electrodes: a nonequilibrium Green's function study[J]. *Physical Review B*, 2005, 72(11): 115438.
- [25] Fisser M, Badcock R A, Teal P D, et al. High-sensitivity fiber-optic sensor for hydrogen detection in gas and transformer oil[J]. *IEEE Sensors Journal*, 2019, 19(9): 3348-3357.
- [26] Ma J, Ju J, Jin L, et al. A compact fiber-tip micro-cavity sensor for high-pressure measurement[J]. *IEEE Photonics Technology Letters*, 2011, 23(21): 1561-1563.
- [27] Li H Y, Lv J M, Li D L, et al. MEMS-on-fiber ultrasonic sensor with two resonant frequencies for partial discharges detection[J]. *Optics Express*, 2020, 28(12): 18431-18439.
- [28] Fong N R, Berini P, Tait R N. Hydrogen sensing with Pd-coated long-range surface plasmon membrane waveguides[J]. *Nanoscale*, 2016, 8(7): 4284-4290.
- [29] Ma J, Jin W, Ho H L, et al. High-sensitivity fiber-tip pressure sensor with graphene diaphragm[J]. *Optics Letters*, 2012, 37(13): 2493-2495.

Fiber-Optic Hydrogen Sensor Based on Palladium-Modified Hexagonal Boron Nitride

Ding Hui, Guo Maosen*, Xu Haodong, Han Chunyang, Chen Chen

School of Electrical Engineering, Xi'an Jiaotong University, Xi'an 710049, Shaanxi, China

Abstract

Objective As a green and renewable energy source, hydrogen (H_2) has caught extensive attention due to its excellent combustion performance and non-polluting characteristics. However, H_2 is a volatile, flammable, and explosive gas that faces risks during its storage, transportation, and utilization. Therefore, the development of online sensors for accurately detecting hydrogen concentration is an effective way to prevent explosive accidents. Fiber-optic hydrogen sensors based on Fabry-Perot (F-P) interferometer have been extensively investigated because of their electromagnetic interference resistance, corrosion resistance, and easy integration. The detection performance of F-P cavity-type fiber-optic hydrogen sensors depends mainly on the characteristics of hydrogen-sensitive films composed of palladium (Pd) and substrate. The results show that the thinner thickness of the Pd leads to faster sensor response, and the thinner thickness of the substrate brings about higher sensor sensitivity. In practice, the thickness of the Pd layer can be controlled by the preparation process, while that of the substrate layer is limited by various factors such as the mechanical strength of the material, and it is difficult to both achieve the desired thickness and ensure the mechanical strength. We propose and fabricate a fiber-optic hydrogen sensor based on Pd-modified hexagonal boron nitride (hBN) films. With the nanoscale thickness and high mechanical strength of hBN, the sensor features high sensitivity, fast response, and excellent repeatability.

Methods We put forward an F-P type fiber-optic hydrogen sensor based on Pd/hBN films. The Pd/hBN film and the fiber end facet act as two partially reflective mirrors, forming a low-finesse flexible F-P interferometer (Fig. 1). When exposed to H_2 , the Pd/hBN film adsorbs and dissociates H_2 molecules. Subsequently, hydrogen atoms diffuse into the Pd film to form PdH_x , which results in the expansion of the Pd lattice and then the deformation of the Pd/hBN film (Fig. 2). The ultrathin Pd film promotes the rapid dissociation of H_2 molecules, and the ultrathin hBN film allows the Pd lattice expansion to be effectively converted into Pd/hBN film displacement, which can be easily measured by fiber-optic interferometry. Theoretical analysis and simulation studies show that the thinner thickness of the hBN film and the larger radius of support structure lead to higher sensor sensitivity (Fig. 4). However, the single-layer hBN film is prone to fracture during the transfer process, and finally a multilayer hBN film is employed as the substrate during sensor

preparation (Fig. 5). The prepared sensor is small and compact, and the output spectrum has a free spectral range of 6.4 nm and an interference fringe contrast of 16 dB (Fig. 6).

Results and Discussions A test platform is built in the laboratory for the test and calibration of the hydrogen sensor (Fig. 7). When the hydrogen volume fraction in the gas chamber is 0.10%, the sensor spectrum shifts toward the short wavelength, and the drift is 0.65 nm after 85 s. During hydrogen desorption, the sensor spectrum shifts toward the long wavelength, and the drift is 0.64 nm after 75 s (Fig. 8). The blue shift and red shift of the sensor spectrum are basically consistent, and the extremely high Young's modulus of hBN equips the Pd/hBN film with good rigidity to ensure that the sensor has no "response memory" problem. The total shift of the dip wavelength near 1537.5 nm is 2.9 nm when the hydrogen volume fraction rises from 0 to 0.50%, the sensitivity obtained by linear fitting is $0.58 \text{ pm}/10^{-6}$, and the detection limit of the sensor is measured to be 30×10^{-6} (Fig. 9). In the three experiments with hydrogen volume fraction of 0.10%, the spectra of the sensor show the same trend, the corresponding blue shifts of the spectra are 0.65 nm, 0.66 nm, and 0.64 nm respectively, and the response time of the sensors is about 60 s for all three experiments (Fig. 10). This is due to the good rigidity and fatigue resistance of the hBN film, which ensures the repeatability of the sensor. The temperature sensitivity of the sensor is $91 \text{ pm}/^{\circ}\text{C}$ (Fig. 11), and the sensor preparation can be improved by bonding to reduce the effect of temperature on the sensor. Compared with other hydrogen sensors based on the Fabry-Perot interferometer, our sensor has a high detection sensitivity (Table 1).

Conclusions A probe type fiber-optic hydrogen sensor with highly sensitive detection characteristics is proposed. The sensor is composed of a flexible Fabry-Perot interferometer with a nanometer-thick hBN as a Pd support film and a single-mode optical fiber. The mechanical and optical properties of the hBN film are discussed, and its significant technical advantages as an F-P interferometer reflective film in mechanical, optical, and hydrogen adsorption/desorption rates are pointed out. The structure of fiber-optic F-P cavity with Pd-modified hBN films as the reflective film is designed and its preparation is studied. Finally, experiments show that the sensor has the detection sensitivity of $0.58 \text{ pm}/10^{-6}$ in the range of hydrogen volume fraction 0.02%–0.50%, the response time of 60 s for the volume fraction of 0.10% hydrogen, and good repeatability. The compact and corrosion-resistant sensor has potential technical advantages in fields such as hydrogen detection in power transformer oil.

Key words sensor; hydrogen volume fraction; boron nitride; Fabry-Perot interference; online measurement